Anal. Bioanal. Electrochem., Vol. 10, No. 3, 2018, 362-371

Analytical & Bioanalytical Electrochemistry

Full Paper

Synthesis of n-type Cu-doped ZnO Nanorods onto FTO by Electrodeposition Method and Study its Electrocatalytic Properties toward CO_2 Reduction

Fazel Ghahramanifard, Ahmad Rouhollahi* and Omid Fazlolahzadeh

Faculty of Chemistry, K.N. Toosi University of Technology, Tehran, Iran

*Corresponding Author, Tel.: (+98) 2285020; Fax: (+98) 2122853650

E-Mail: Rouhollahi@kntu.ac.ir

Received: 23 September 2017 / Accepted with minor revision: 15 November 2017 / Published online: 31 March 2018

Abstract- n-type Copper-doped zinc oxide nanorods (CZO NRs) were electrodeposited on fluorine-doped tin oxide (FTO) substrates at low temperature. Nanorod array morphology with wurtzite hexagonal structure was characterized by SEM and XRD. XRD patterns show CZO NRs growth along c-axis perpendicular to the plane of the glass substrate and Cu^{2+} ions substituted with Zn^{2+} ions and did not change the hexagonal wurtzite structure of the ZnO nanorods. EDX spectra show the presence of Cu in the sample. UV-Vis spectra indicate optical band gap of ZnO narrow by Cu doping. Mott-Schottky analysis reveals that prepared CZO NRs has n-type conductivity. Voltammetry analysis shows CZO NRs have the electrocatalytic activity toward CO_2 reduction at

Keywords- ZnO nanorods, Carbon dioxide, Mott-Schottky, Electrodeposition

1. INTRODUCTION

In the past decade, metal oxide semiconductors have been attracted considerable attention for photocatalytic degradation of pollutants and clean energy production [1]. ZnO and TiO_2 are two promising metal oxide semiconductors in photocatalytic and photovoltaic applications. Both of them are n-type and their band gap, conduction, and valence band edge positions are similar [2]. ZnO with a direct band gap of 3.37 eV at room temperature has

several advantages in comparison to TiO_2 [3]. ZnO absorbs a large fraction of solar spectrum than TiO_2 [4] and also possesses higher electron mobility and point defects oriented from oxygen vacancies [5]. Also, its chemical reactivity is higher than TiO_2 and can be synthesized at lower temperature [6]. In addition, ZnO can form a variety of nanostructures including nanotubes, nanowires, nanobelts, nanoflowers, nanospheres, nanobowls, nanocombs, nanotetrapods and nanorods [7], in which one-dimensional (1D) ZnO nanostructures such as nanobelts, nanotubes, nanowires, and nanorods are suitable materials for photoelectrode of photoelectrochemical (PEC) systems due to their efficient charge transport, high specific surface area, high light absorption, surface defects, and oxygen vacancy [8]. In recent years, ZnO nanomaterials are widely used as photocatalysts for degradation of toxic dyes and environmental hazardous pollutants such as phenol [9], direct blue15 [10] due to its low cost, non-toxic, stability, inertness and unique optoelectronic property [2,4]. Large band gap and high recombination rate of photogenerated electron/hole are two major drawbacks of ZnO that persuade us to modify it. Metal doping into ZnO is a straightforward strategy for resolving these problems [11].

Recently our group reported Cu ion doping at low concentration ($[Cu^{2+}]/[Zn^{2+}]$=0.5 and 1.0 at. % in deposition bath) into ZnO nanorods by electrodeposition method not only reduce its optical band gap from UV region to visible but also reduce charge recombination rate of electron/hole [12]. Furthermore, our experimental data shows doped Cu ions can act as acceptors and change conductivity from n-type to p-type. With this achievement, Cu-doped p-ZnO can be used successfully as photocathode in CO_2 photoelectroreduction and H_2O splitting. It should be noted that construction of stable p-type ZnO is a challenging subject. Cui et al. [13] reported that conductivity of electrodeposited Ag-doped ZnO nanowires depends on dopant concentration.

In this study, we investigate the effect of excess concentration of Cu ion dopant ($[Cu^{2+}]/[Zn^{2+}]$=1.5 at. %) on structural, optical band gap, conductivity and catalytic properties of ZnO nanorods.

2. EXPERIMENTAL

2.1. Preparation of CZO NRs

CZO NRs prepared on the transparent conductive glass (FTO) by two-step potentiostatic method as reported previously [12]. Deposition bath contains aqueous solution of 1.0 mM $Zn(NO_3)_2.6H_2O$, 1.0 mM HMTA (hexamethylenetetramine), 0.1 M $NaNO_3$ and 0.015 mM $CuSO_4$. Electrochemical depositions were performed using an Autolab PGSTAT30 potentiostat/galvanostat connected to the PC and running by GPES 4.9 software.

2.2. Characterization

X-ray diffraction (XRD) patterns of the sample were recorded by PANalytical XPert Pro MPD with a monochromatizes Cu Kα irradiation (λ=1.5406 Å). Surface morphology was examined by scanning electron microscopy (SEM) (Philips XL30). Elemental analysis of the sample was performed using energy-dispersive X-ray spectroscopy (EDS) (VEGA3 LM/Tescun Company). UV-Vis spectra were recorded at room temperature by Shimadzu spectrophotometer with D_2-W lamps.

2.3. Electrochemical measurement

Electrochemical experiments were carried in a conventional single compartment sealed glass cell with a three-electrode configuration powered by an electrochemical system consisting of a potentiostat/ galvanostat (Autolab PGSTAT30) which was run by a PC through the GPES 4.9 software. The working electrode was CZO NRs, the counter electrode was a Pt wire, and an Ag/AgCl wire acted as the quasi-reference electrode. The Ag/AgCl quasi-reference electrode is calibrated using ferrocene/ferrocenium redox couple as an internal reference, and all potentials converted to the NHE (Normal Hydrogen Electrode) reference scale. All measurements were done in acetonitrile containing 0.1 M tetrabutylammonium hexafluorophosphate (TBAHP) as supporting electrolyte at 298±2K. The light source was a conventional white LED light in the visible region (6000 K, 100 W) and the light intensity on the reaction vessel was found to be 5 mW/cm^2.

3. RESULTS AND DISCUSSION

3.1. Electrochemical deposition of CZO

It is well-established that the first step in electrodeposition of ZnO from $Zn(NO_3)_2$ is the reduction of nitrate ions to hydroxide [14]. To choose the appropriate potential for electrodeposition, cyclic voltammogram (CV) scan of bare FTO in solution bath containing precursor were recorded. As shown in Fig. 1, in deposition bath (zinc nitrate, HMTA and $NaNO_3$), a cathodic wave starting at -1 V *vs* Ag/AgCl with a maximum current density of 0.5 mA/cm^2 appear which can be assigned to the electrochemical reduction of nitrate ions. However, this wave shifts toward positive direction with enhanced current density when copper ions present in solution (Fig. 1 b and c) demonstrates the catalytic effect of cuprous ions on nitrate reduction [15]. As a result, -1 V *vs*. Ag/AgCl was chosen as electrodeposition potential for synthesis of CZO NRs by chronoamperometry (potentiostat) method.

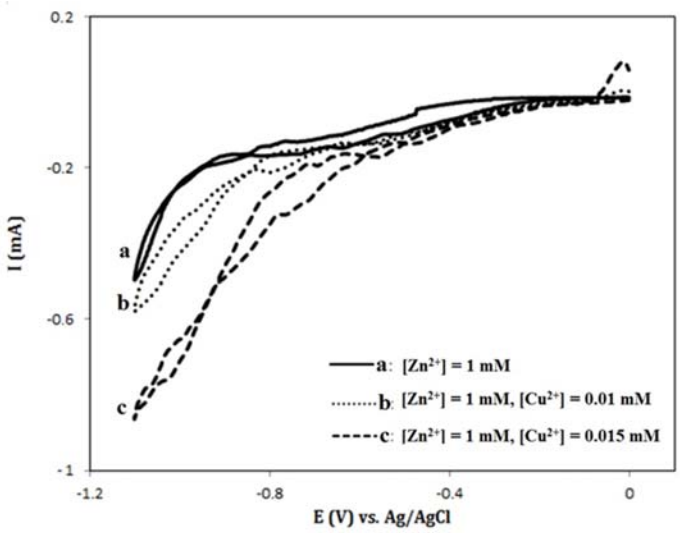

Fig. 1. Cyclic voltammograms of bare FTO in deposition bath containing (a) $[Cu^{2+}]$=0, (b) $[Cu^{2+}]$=0.01 mM, and (c) $[Cu^{2+}]$=0.015 mM. In all experiments ($Zn(NO_3)_2$=1 mM, HMTA=1 mM, T=80 ´C, scan rate=30 mV/s, counter electrode: Pt wire, reference electrode: Ag/AgCl.

3.2. XRD, SEM and EDS characterizations

Fig. 2 shows XRD patterns of the sample in which narrow and sharp peaks indicating good crystalline characteristics of the samples. The observed patterns related to the wurtzite hexagonal phase of ZnO and showing good agreement with the data of the Joint Committee on Powder Diffraction Standards (JCPDS) card no. 36-1451 [16]. Strong (002) peak indicate preferential growth along c-axis perpendicular to the plane of the glass substrate.

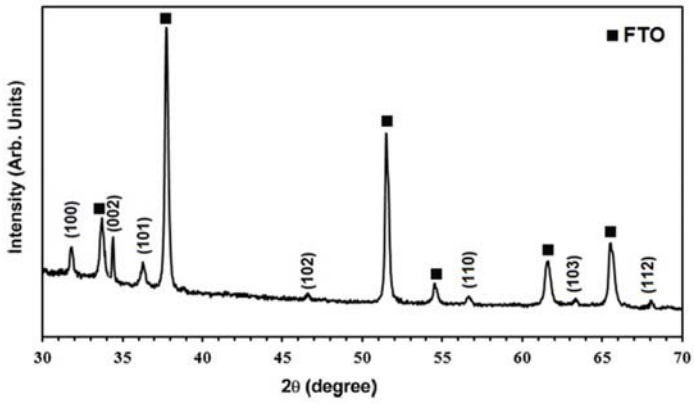

Fig. 2. XRD patterns of CZO NRs at room temperature

Table 1. The peak position of (002) plane, lattice parameter "a" and "c", c/a ratio, bond length (l), volume (V), average crystal size (D), and stress (σ) of CZO NRs

Samples	**2θ(˚) (002)**	**Lattice parameters (Å)**		**c/a ratio**	**Bond length in in c-axis direction (Å)**	**Bond length in other two directions (Å)**	**Volume, V (Å)^3**	**D (average) (nm)**	**Stress, σ (GPa)**
		a=b	**C**						
CZO NRs	34.420	3.2467	5.2074	1.6039	1.9762	1.9767	47.5357	37	-0.089

Fig. 3 shows the typical top view SEM images of the electrodeposited sample at different magnifications. Low–magnification SEM image shows vertically well-aligned nanorods growth throughout the substrate surface. From the high–magnification SEM image it can be clearly observed that all nanorods contained flat surface with a hexagonal shape which had an average diameter around 100–150 nm. High–magnification image shows that hexagonally CZO NRs are poorly ordered due to the substitution of Zn^{2+} ions by smaller Cu^{2+} ions. Similarly, it has been reported that during growth of ZnO NRs, Cu ions can enhance the growth rate and hence coalescence process for nanorods by increasing the density of nucleation site [19].

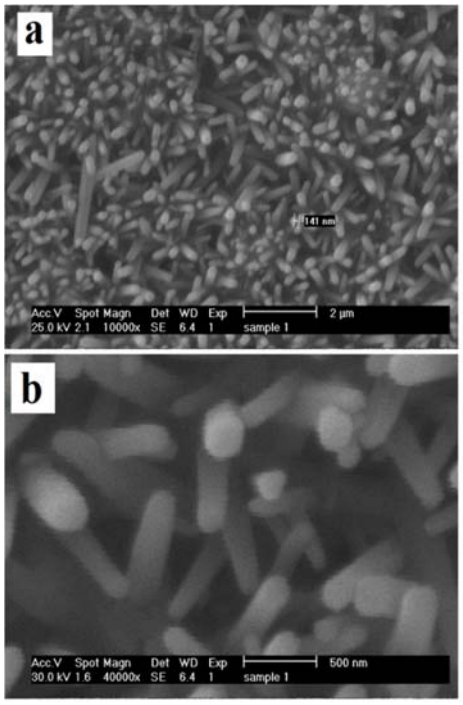

Fig. 3. SEM images of CZO NRs at (a) low and (b) high magnification

EDS spectra (Fig. 4) shows the incorporation of Cu into ZnO NRs. Also, the ratio of [Cu]/[Zn] (10.1%) was higher than that in the deposition bath (1.5%).

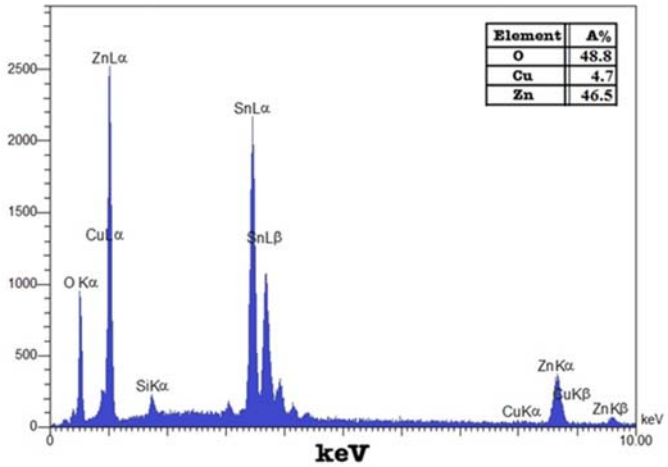

Fig. 4. EDS spectra of CZO NRs. (Si, Sn and Au signals arise from the glass substrate, FTO, and Au was coated on samples)

3.3. Optical property and band gap analysis

In order to study the optical properties of CZO NRs, absorption spectra of the sample were recorded in the wavelength range of 300–800 nm using UV-Vis spectrophotometer at room temperature, as shown in Fig. 5(a). As can be seen, CZO NRs has considerable absorption in the visible region. However, pure ZnO only absorbs UV lights, the absorption edge of CZO is in the visible region. It seems that, by Cu incorporation, the optical band gap exhibits a gradual redshift.

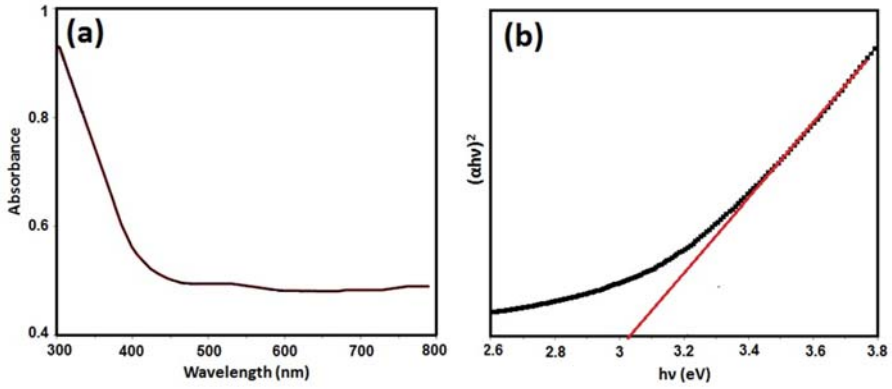

Fig. 5. (a) UV-visible absorption spectra of CZO NRs, and (b) plot of $(\alpha h\nu)^2$ *vs.* hν

The optical band gap of samples was further evaluated using the Tauc formula (eq. 1) [20]:

$$\alpha h\upsilon = A\left(h\upsilon - E_g\right)^n \quad (1)$$

Where α is absorption coefficient, A is constant, E_g is the optical band gap, hυ is the photon energy and n is an index. By applying n=1/2, the optical band gap of CZO NRs was found 3.04 eV, as can be seen in Fig. 5(b). The narrowing optical band gap of ZnO by Cu doping is consistent with the earlier report by Sharma et, al. [20]. The reduction in optical band gap with Cu doping is originated from the strong d–p hybridization between Cu and O which moves up the 2p orbitals of O [21].

3.4. Mott-Schottky analysis

In order to obtain further information about semiconductors such as conductivity, flat band potential and charge carrier density, the Mott-Schottky analysis carried out. The Mott–Schottky equation is based on the space charge capacitance obtained from impedance spectroscopy and can be described as follows (Eq. 2) [22]:

$$\frac{1}{C^2} = \left(\frac{2}{e_0 \varepsilon \varepsilon_0 N}\right)\left(\left(V_{app} - V_{fb}\right) - \frac{kT}{e_0}\right) \quad (2)$$

Where C is the capacitance between photoelectrode and electrolyte, e_0 is the electron charge, ε is the dielectric constant of ZnO (ε=8), ε_0 denotes the permittivity of free space, N is the charge carrier density, V represents the applied electrode potential, V_{fb} is the flat band potential, k is the Boltzmann constant, and T is the absolute temperature.

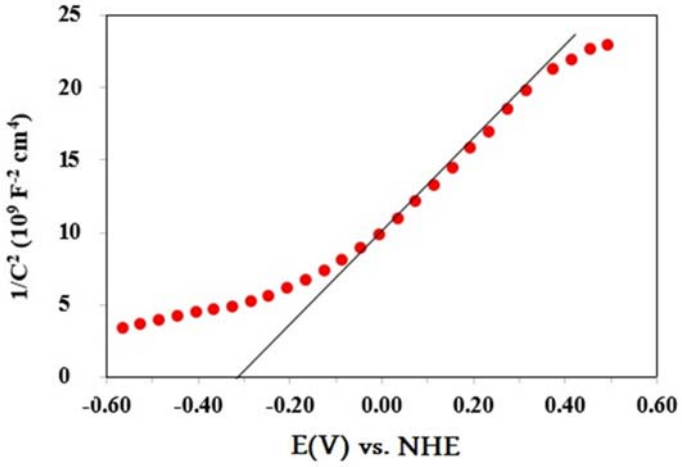

Fig. 6. Mott-Schottky plot of CZO NRs

As shown in Fig. 6, Mott-Schottky plot of CZO NRs has a positive slope, indicates this sample is an n-type semiconductor. Although in our previous study [12], when the ratio of $[Cu^{2+}]/[Zn^{2+}]$=0.5 and 1.0 at. % in the electrodeposition bath, conductivity is p-type. This

observation is in good agreement with Cuis report [13] for Ag-doped ZnO nanowires. This behavior can be explained as follows: Increasing the dopant concentration disrupts the normal ZnO growth process and produces more hole–killer defects. Furthermore, flat band potential and charge carrier density of CZO NRs calculated -0.32 V *vs* NHE and 5.4×10^{20} cm^{-1}, respectively. The value of donor density is three orders of magnitude higher than that of ZnO prepared by chemical method [23].

3.5. Voltammetry analysis

To study the electrochemical and photoelectrochemical activity of CZO NRs electrodes toward CO_2 reduction, linear sweep voltammetry (LSV) experiments were conducted in acetonitrile containing 0.1 M TBAHP (as supporting electrolyte) saturated with either N_2 or CO_2 in dark and under illuminated conditions (Fig. 7). In dark and N_2 saturated solution, CZO NRs electrodes show large background current as the potential is scanned in the negative direction due to the presence of surface states created by Cu doping [24]. Comparison between LSVs record in dark and under illumination conditions, no significant photocurrent observed, indicating CZO NRs is n-type semiconductors and under negative bias, create accumulation layer.

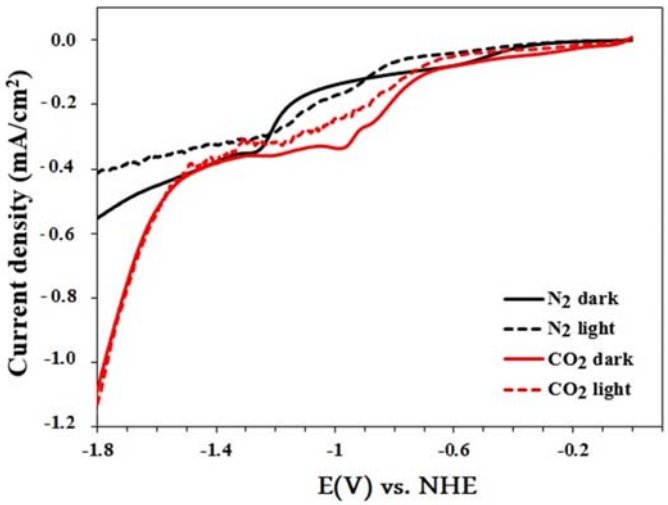

Fig. 7. Linear sweep voltammograms obtained for CZO NRs in N_2 (black) and CO_2 (red)-saturated solutions in darkness (solid line) and under visible light (dotted line). Conditions: 0.1 M TBAHP/acetonitrile; Pt counter electrode; Ag/AgCl quasi-reference electrode; referenced to internal ferrocene standard; scan rate 50 mV/s

Due to recombination losses in the surface states at the electrode/liquid interface, the photocurrent onset potential observed in LSV is different from potential obtained by Mott–Schottky equation [24]. In dark and CO_2 saturated solution, LSVs show significant reduction

current density relative to that obtained with an N_2–saturated solution at onset potential of -0.7 V *vs* NHE corresponding CO_2 reduction. It indicates that Cu doping improves electrocatalytic CO_2 reduction activity of CZO NRs which can be attributed to the presence of Cu species on the surface that provides more adsorption sites for CO_2 molecules [25]. As expected, the photocurrent and dark current of CZO NRs is the same in CO_2 saturated solution, due to the n-type conductivity of CZO NRs that acts as a metallic electrode (dark cathode) at potentials more negative than flat band potential. Furthermore in CO_2 saturated solution in dark LSV show three peaks within the potential range from -0.8 to -1.1 V which can be attributed to further reduction of intermediate and adducts. While under light illumination these waves disappear because charge carrier concentration and electrode/electrolyte interface property change under light. This experiment reveals Cu-doped n-ZnO has electrocatalytic activity toward CO_2 reduction. However, as expected, the n-type semiconductor has no significant photoelectroreduction activity.

4. CONCLUSION

In summary, n-type Cu-doped ZnO NRs were electrodeposited on FTO glass by facile and simple electrochemical method at low temperature. By electrodeposition route, Cu ions was successfully doped in substitutional positions instead of Zn^{2+} in hexagonal wurtzite structure of ZnO NRs. Doped Cu ions can reduce optical band gap of ZnO from UV region to visible due to strong d-p hybridization between Cu and O which moves up O 2p and narrowing the band gap. At low concentration of Cu ions, Cu can act as acceptor and induce p-type conductivity, but in this work [Cu]/[Zn]=10.1%, substituted Cu ions act as donor center and induce n-type conductivity with high donor density because increasing Cu ion concentration disrupts the normal ZnO growth process and produces more hole-killer defects and induces n-type conductivity. In acetonitrile solvent, Cu doped ZnO NRs electrode shows electrocatalytic activity toward CO_2 reduction at less overpotential with high current density due to the existence of Cu species on ZnO surface which provide more adsorption site for CO_2 molecules.

REFERENCES

[1] Y. Y. Lee, H. S. Jung, and Y. T. Kang, J. CO_2 Util. 20 (2017) 163.

[2] A. Senthilraja, B. Subash, B. Krishnakumar, M. Swaminathan, and M. Shanthi, Superlattices Microstruct. 75 (2014) 701.

[3] A. Simimola, P. Chowdhurya, S. K. Ghoshb, and H. C. Barshilia, Electrochim. Acta 90 (2013) 514.

[4] O. Lupan, T. Pauporte´, L. Chow, B. Vian, F. Pelle´, L. K. Ono, B. Roldan Cuenya, and H. Heinrich, Appl. Sur. Sci. 256 (2010) 1895.

[5] I. Udom, M. Ram, E. K. Stefanakos, A. Hepp, and D. Y. Goswami, Mater. Sci. Semicond. Process. 16 (2013) 2070.
[6] Asdim, K. Ichinose, T. Inomata, H. Masuda, and T. Yoshida, J. Photochem. Photobiol. A 242 (2012) 67.
[7] S. Magdalena, and Z. Kamila, Electrochim. Acta 127 (2014) 467.
[8] [8] C. Hsien-Ming, Y. Tung-Han, H. Yang-Chih, P. Tsong-Pyng, and W. Jenn-Ming, Appl. Catal. B-Environ. 163 (2015) 156.
[9] G. S. Claudia, J. S. Maria, A. C. Sonia, and W. L. O. Joao, J. Catal. 316 (2014) 182.
[10] L. Randeep, U. Ahmad, S. K. Mehta, and K. K. Sushil, Talanta 131 (2015) 490.
[11] L. Jia, W. Huihu, D. Shijie, W. Fanqiang, and D. Yifan, J. Alloys Compd. 617 (2014) 869.
[12] F. Ghahramanifard, A. Rouhollahi, and O. Fazlolahzadeh, Superlattices Microstruct. 114 (2018) 1.
[13] A. Thomas, and J. B. Cui, J. Phys. Chem. Lett. 1 (2010) 1090.
[14] I. Masanobu, J. Electrochem. Soc. 146 (1999) 4517.
[15] E. V. Filimonov, and A. I. Shcherbakov, Protect. Metal. 40 (2004) 280.
[16] M. Ashokkumar, and S. Muthukumaran, Opt. Mater. 37 (2014) 671.
[17] X. Peng, J. Xu, H. Zang, B. Wang, and Z. Wang, J. Lumin. 128 (2008) 297.
[18] G. Sigircik, O. Erken, T. Tuken, C. Gumus, O. M. Ozkendir, and Y. Ufuktepe, Appl. Surf. Sci. 340 (2015) 1.
[19] A. K. Singh, G. S. Thool, R. S. Singh, and S. P. Singh, J. Alloys Compd. 618 (2015) 421.
[20] M. Mittal, M. Sharma, and O. P. Pandey, Sol. Energy 110 (2014) 386.
[21] S. S. Xu, H. L. Lu, Y. Zhang, T. Wang, Y. Geng, W. Huang, S. J. Ding, and D. W. Zhang, J. Alloys Compd. 638 (2015) 133.
[22] M. Radecka, M. Rekas, A. Trenczek-Zajac, and K. Zakrzewska, J. Power Sources 181 (2008) 46.
[23] R. C. Pawar, S. H. ShaikJ, A. A. Babar, P. M. Dhere, and P. S. Patil, Sol. Energy 85 (2011) 1119.
[24] P. Chhetri, K. K. Barakoti, and M. A. Alpuche-Aviles, J. Phys. Chem. C 119 (2015) 1506.
[25] D. Sahu, N. R. Panda, B. S. Acharya, and A. K. Panda, Ceram. Int. 40 (2014) 11041.